

This is an Open Access document downloaded from ORCA, Cardiff University's institutional repository:<https://orca.cardiff.ac.uk/id/eprint/141487/>

This is the author's version of a work that was submitted to / accepted for publication.

Citation for final published version:

Kwan, D. C. M., Kesaria, M. , Anyebe, E. A. , Alshahrani, D. O., Delmas, M. , Liang, B. L. and Huffaker, D. L. 2021. Optical and structural investigation of a 10 μm InAs/GaSb type-II superlattice on GaAs. *Applied Physics Letters* 118 (20) , 203102. 10.1063/5.0045703

Publishers page: <http://dx.doi.org/10.1063/5.0045703>

Please note:

Changes made as a result of publishing processes such as copy-editing, formatting and page numbers may not be reflected in this version. For the definitive version of this publication, please refer to the published source. You are advised to consult the publisher's version if you wish to cite this paper.

This version is being made available in accordance with publisher policies. See <http://orca.cf.ac.uk/policies.html> for usage policies. Copyright and moral rights for publications made available in ORCA are retained by the copyright holders.



Optical and structural investigation of a 10 μm InAs/GaSb type-II superlattice on GaAs

Cite as: Appl. Phys. Lett. **118**, 203102 (2021); <https://doi.org/10.1063/5.0045703>

Submitted: 28 January 2021 . Accepted: 04 May 2021 . Published Online: 20 May 2021

 D. C. M. Kwan,  M. Kesaria,  E. A. Anyebe, D. O. Alshahrani, M. Delmas,  B. L. Liang, and D. L. Huffaker



View Online



Export Citation



CrossMark

ARTICLES YOU MAY BE INTERESTED IN

Long wavelength InAs/InAsSb superlattice barrier infrared detectors with p-type absorber quantum efficiency enhancement

Applied Physics Letters **118**, 133503 (2021); <https://doi.org/10.1063/5.0047937>

Low noise $\text{Al}_{0.85}\text{Ga}_{0.15}\text{As}_{0.56}\text{Sb}_{0.44}$ avalanche photodiodes on InP substrates

Applied Physics Letters **118**, 081106 (2021); <https://doi.org/10.1063/5.0035571>

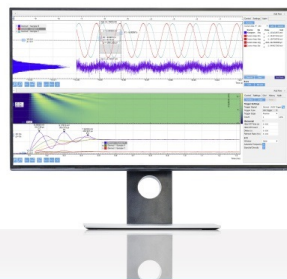
All-epitaxial guided-mode resonance mid-wave infrared detectors

Applied Physics Letters **118**, 201102 (2021); <https://doi.org/10.1063/5.0047534>

Challenge us.

What are your needs for
periodic signal detection?

Watch 



Zurich
Instruments

Optical and structural investigation of a $10\ \mu\text{m}$ InAs/GaSb type-II superlattice on GaAs

Cite as: Appl. Phys. Lett. **118**, 203102 (2021); doi: [10.1063/5.0045703](https://doi.org/10.1063/5.0045703)

Submitted: 28 January 2021 · Accepted: 4 May 2021 ·

Published Online: 20 May 2021



View Online



Export Citation



CrossMark

D. C. M. Kwan,¹ M. Kesaria,^{1,a)} E. A. Anyebe,² D. O. Alshahrani,¹ M. Delmas,^{1,b)} B. L. Liang,³ and D. L. Huffaker^{1,b,c)}

AFFILIATIONS

¹School of Physics and Astronomy, Cardiff University, The Parade, Cardiff CF24 3AA, United Kingdom

²School of Engineering, Cardiff University, The Parade, Cardiff CF24 3AA, United Kingdom

³California NanoSystems Institute, University of California, Los Angeles, California 90095, USA

^{a)}Author to whom correspondence should be addressed: kesariam@cardiff.ac.uk

^{b)}Present address: IRnova AB, Electrum 236 - C5, SE-164 40 Kista, Sweden.

^{c)}Present address: Electrical Engineering Department, The University of Texas at Arlington, Arlington, TX 76019, USA.

ABSTRACT

We report on a $10\ \mu\text{m}$ InAs/GaSb type-II superlattice (T2SL) grown by molecular beam epitaxy on a GaAs substrate using an interfacial misfit (IMF) array and investigate the optical and structural properties in comparison with a T2SL grown on a GaSb substrate. The reference T2SL on GaSb is of high structural quality as evidenced in the high-resolution x-ray diffraction (HRXRD) measurement. The full width at half maximum (FWHM) of the HRXRD peak of the T2SL on GaAs is 5 times larger than that on GaSb. The long-wave infrared (LWIR) emission spectra were analyzed, and the observed transitions were in good agreement with the calculated emission energies. The photoluminescence (PL) intensity maxima (I_{\max}) of $\sim 10\ \mu\text{m}$ at 77 K is significantly reduced by a factor of 8.5 on the GaAs substrate. The peak fitting analysis of the PL profile indicates the formation of sub-monolayer features at the interfaces. PL mapping highlights the non-uniformity of the T2SL on GaAs which corroborates with Nomarski imaging, suggesting an increase in defect density.

Published under an exclusive license by AIP Publishing. <https://doi.org/10.1063/5.0045703>

Electromagnetic radiation around $10\ \mu\text{m}$ in wavelength contains information about our environment which is vital for defence, earth observation, and biological imaging applications. The black body radiation maximum at room temperature is around $10\ \mu\text{m}$; hence, it is challenging for detectors aimed at this wavelength to achieve the state-of-the-art background limited infrared photodetection (BLIP). This drives the demand for detectors with extreme high-temperature sensitivities to distinguish between target and background objects. HgCdTe (MCT) is the preferred material system for $10\ \mu\text{m}$ detectors but drawbacks such as the cost and availability of substrates and fabrication difficulties have motivated the search for an alternative. Also, the restriction of hazardous substances (RoHS) directive limits the utilization of heavy metals such as Hg, Cd, and Te in electrical and electronic equipment under EU legislation.¹ Hence, there is an urgent need to develop an alternative to MCT. For this wavelength, group III-V quantum well-infrared photodetectors (QWIPs) and type-II superlattice (T2SL) detectors are the competitive technologies. Due to the inherent interband transition, QWIPs are limited to a narrow spectral band and low

quantum efficiency (<10%). T2SLs of InAs/GaSb have, since their conception in 1977,² been increasingly viewed as a promising candidate for $10\ \mu\text{m}$ detectors,^{3–6} due to reduction of Auger recombination,^{7,8} reduced tunneling currents,⁹ and development of novel device architectures such as nBn to reduce the dark current.^{10–15} Despite these theoretical advantages, T2SLs have yet to demonstrate improved device performance compared to MCT. In the present scenario, there is a shift from conventional GaSb to GaAs substrates due to their size, availability, low cost, and semi-insulating properties. Furthermore, transparency in the long-wave infrared (LWIR) regime enables the fabrication of backside-illuminated devices which can make use of monolithically integrated immersion lenses (ILs). This technique increases the optical area of the detector in comparison with its electrical size and has allowed LWIR T2SLs to achieve larger detectivities than MCT at temperatures above $\sim 210\text{ K}$ ^{16–21} though this presents difficulties for scaling to focal plane arrays (FPAs). The difference in refractive index between the InAs/GaSb T2SL and GaAs is also believed to increase the quantum efficiency of devices on GaAs substrates.²²

InAs/GaSb T2SLs photodiodes have been demonstrated in both mid-wavelength infrared (MWIR)²³ and LWIR^{22,24} spectral ranges on the GaAs substrate. It is clear from these examples that the 7.3% lattice mismatch between the superlattice and the substrate led to a degradation in material quality and limited the performance of the photodiode. To maintain the material quality of antimonides on GaAs, Huffaker *et al.*²⁵ have demonstrated the interfacial misfit (IMF) array at the GaSb-on-GaAs interface (IF) in which periodic 90° misfit dislocations prevent the propagation of threading dislocations. Despite the increasing popularity of antimonides on GaAs substrates and the efficacy of the IMF array, many studies suggest degradation of device performance which is attributed to the heteroepitaxial growth.^{26–28} This has led to the widespread use of alternative strain compensation techniques such as metamorphic buffer layers,^{20,29,30} dislocation filters,^{31–33} low-temperature nucleation,^{23,29} and 3D growth islands.^{32,33} These techniques, and any combination thereof, usually require the use of a thick buffer layer and have so far demonstrated only limited improvement in device performance. This suggests that there is a need to investigate the structural and optical quality of 10 μm wavelength T2SLs on GaAs to improve epi-quality and allow the growth of thick, high-quality T2SLs on GaAs with performance comparable to T2SLs on GaSb. Previously reported optical studies of LWIR T2SLs on GaAs substrates do not directly make a comparison with a reference sample grown on GaSb, thus making any insights they offer on the change of substrates less informative.^{34–36} Furthermore, the majority of studies on GaAs ILs for T2SLs have been on the InAs/InAsSb variant largely due to its inherent defect tolerance.^{16–21} However, the advantages of InAs/GaSb T2SLs in LWIR, such as stronger absorption and better hole transport properties, suggest that this material system is comparatively understudied.

In a previous work, we have demonstrated a 12 monolayer (ML) InAs/4 ML GaSb SL structure suitable for high-performance LWIR detector applications.³⁷ This Letter compares the optical and structural quality of two 12/4 SLs on GaSb and GaAs substrates. The proposed study seeks to investigate the effect of transferring T2SLs from GaSb to GaAs substrates on the structural and optical quality which were

investigated by high-resolution x-ray diffraction (HRXRD) and photoluminescence (PL), respectively. Ultimately, the results can be used to optimize the design and growth of T2SLs on GaAs in which the non-native substrate does not diminish device performance.

The samples in this study were grown by Molecular Beam Epitaxy (MBE) in a Veeco Gen 930 MBE reactor equipped with dual filament SUMO Knudsen effusion cells for Ga and In and Mark B valved cracker effusion cells for As and Sb. The In and Ga growth rates were set to 0.3 and 0.5 ML s⁻¹, respectively. The InAs and GaSb layers were grown using a V/III flux ratio calibrated from RHEED oscillations of 1.2 and 2, respectively. Both SL samples were grown under the same growth conditions. A reference sample (sample A) was grown on a quarter of a two-inch p-type (0 0 1) GaSb substrate as described in Ref. 37. The second sample (sample B) was grown on a quarter of a two-inch semi-insulating GaAs (1 0 0) substrate. A 500 nm GaSb buffer layer was grown with an IMF array at the GaSb-on-GaAs IF followed by 80 periods of 12/4 SL layer capped with 4 ML of GaSb. A strain compensating interfacial InSb layer was intentionally grown at the interfaces for both samples using migration enhanced epitaxy.³⁸ HRXRD measurements were performed using a Bede D1 x-ray diffractometer. To perform PL measurements, the samples were loaded into a liquid nitrogen cooled cryostat equipped with CaF₂ windows. A pattern generator was used to modulate the excitation source, a 785 nm diode laser, at a frequency of 20 kHz, and a lock-in amplifier was then used to subtract the background signal. A Nicolet iS50-R Fourier Transform Infrared Spectrometer (FTIR), equipped with a KBr beam splitter and liquid nitrogen cooled MCT-A detector, was used to collect the signal.

Figure 1(a) depicts the $\omega/2\theta$ HRXRD pattern of samples A and B and (b) shows a slight mismatch of ~60 arc sec between the substrate and superlattice layers of sample A. The zeroth-order satellite peak of sample A and B overlaps with the GaSb peak, indicating that the superlattice layers are nearly lattice-matched onto the GaSb substrate and GaSb buffer layer for samples A and B, respectively. Sample A displays the sharpest satellite peaks with narrow full width at half maximum (FWHM) which is ~5x smaller than that of Sample B. This

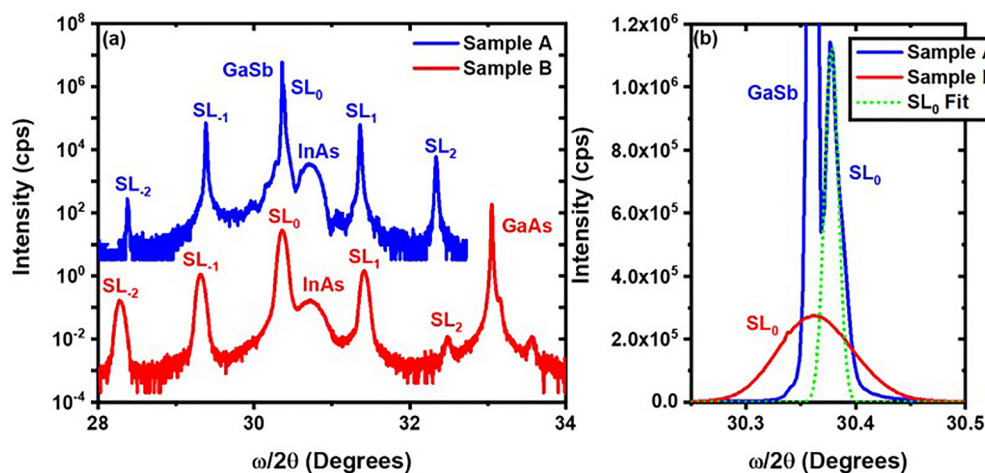


FIG. 1. (a) HRXRD pattern for samples A and B, the zeroth-order satellite peak of sample B is aligned with sample A for clarity. (b) The enhanced plot of the SL_0 peak of sample A and B with a Gaussian fit highlighting SL_0 for sample A, the GaSb substrate peak of sample A is also visible.

TABLE I. Parameters extracted from the analysis of HRXRD patterns.

Sample	Substrate	FWHM SL ₁ (arcsec)	Period thickness (nm)
Sample A	GaSb	60	5.17
Sample B	GaAs	301	4.87

could be associated with the degradation of material quality caused by the regeneration of threading dislocations.³⁹ Table I shows the measured period thickness of sample A is larger than that of sample B; however, both values are close to the expected thickness of ~ 5 nm for the 12/4 SL with InSb IFs. The slight disparity in period thickness may be attributed to uncertainty in the SL IFs or a change in composition.^{40,41}

Normalized PL spectra between 77 and 240 K for Samples A and B are shown in Figs. 2(a) and 2(b), respectively. The dominant PL peak at around 0.11–0.13 eV (77 K) is attributed to the primary electron miniband to first heavy hole miniband (e_1 -hh₁) transition (indicated with dashed lines to serve as a guide). A redshift is observed with increasing temperature for both samples which is consistent with previous reports^{37,38} and attributed to the lattice thermal expansion.⁴²

An 8-band k·p solver, implemented in the Nextnano3 software, was used to model the band structure of the 12 ML InAs/4 ML GaSb T2SL. The model, including the parameters used, is described in detail

in Ref. 43. The results are illustrated in Figs. 2(c) and 2(d). The calculated energy gap of 121 meV at 77 K is close to that measured by PL. The difference can be accounted for by the uncertainty of the interfacial layer as discussed below.

Figure 3(a) shows the integrated PL intensity of as-grown samples as a function of laser power. A peak fitting method described below was used to consider only the e_1 -hh₁ peak. The data were fitted using the equation⁴⁴

$$I_{PL} = aP^\beta, \quad (1)$$

where I_{PL} is the integrated PL intensity, P is the power of the pump laser, a is a constant, and β is the gradient of the slope related to the dominant recombination process. Note that the anomalous reading at 60 mW for sample B has been omitted from the fit. A value of $\beta = 1/2$, 1, or 3/2, indicates the dominant recombination mechanism is Shockley–Read–Hall (SRH), radiative or Auger related, respectively. The gradient, β , was found to be 0.99 for sample A which indicates that radiative recombination is the dominant recombination process and confirms the good crystalline quality of this sample. The gradient for sample B was found to be 1.25, indicating that both radiative and Auger recombination processes are present in this sample. Previous studies have shown that LWIR Ga-containing T2SLs are dominated by non-radiative SRH processes.^{45,46} However, recombination is known to be highly sensitive to factors, such as SL composition, strain and doping concentration, and polarity. The minority carrier lifetime,

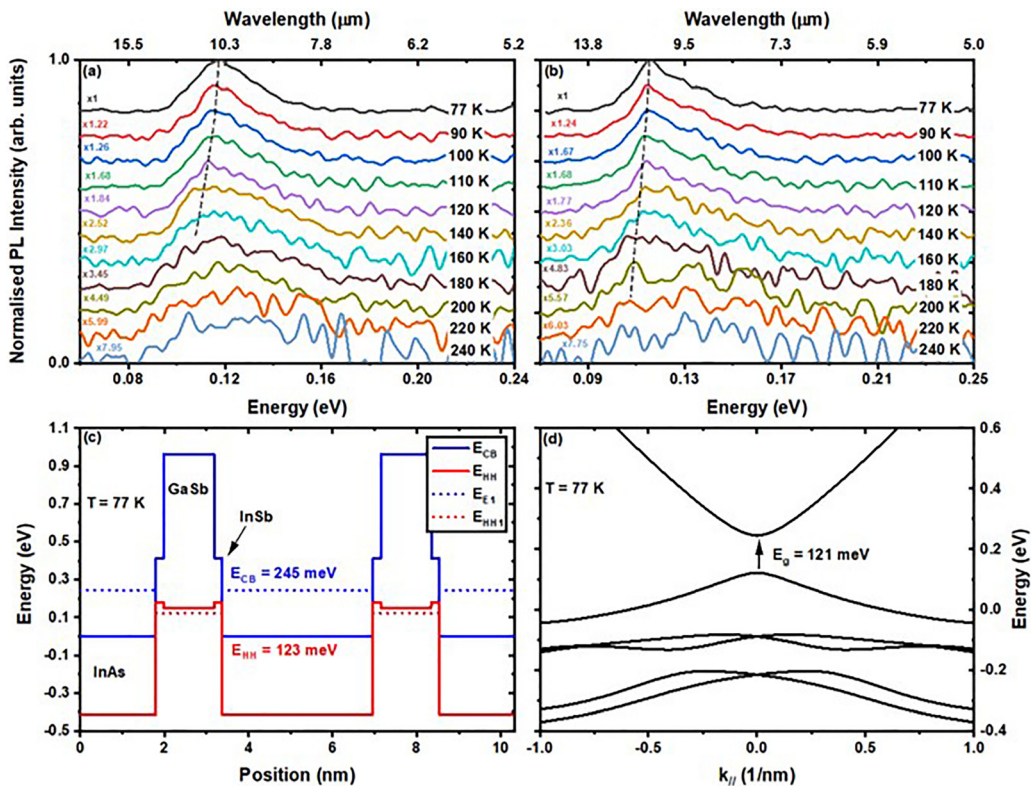


FIG. 2. Normalized PL spectra for (a) sample A and (b) sample B from 77–240 K. (c) A schematic diagram of the simulated band structure of the 12/4 SL including the interfacial InSb layer. (d) The $E(k)$ diagram for the in-plane direction in the Brillouin zone k_{\parallel} .

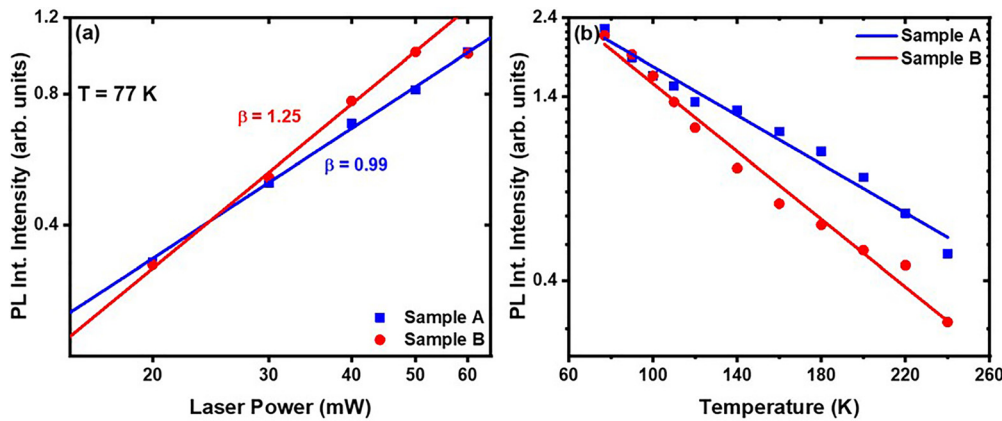


FIG. 3. (a) The integrated PL intensity for sample A and B for (a) different laser excitation powers at 77 K and (b) as a function of temperature.

τ , is the sum of SRH, radiative and Auger recombination contributions.⁴⁵ The contributions of radiative and Auger processes can be neglected for low excess carrier density, δn , but become increasingly significant when δn increases. It is, therefore, possible that the disparity between our results and those recorded in literature arises from a disparity in the excess carrier density. The presence of Auger recombination in sample B is also notable as it contradicts theoretical analysis arguing for the suppression of Auger processes in type-II structures. However, recent modeling performed by Klipstein *et al.*⁴⁷ suggests the existence of an effective Auger recombination process in Ga-containing T2SLs. The presence of Auger recombination in sample B and not sample A may be attributed to the lower bandgap of sample B as Auger coefficients are generally exponentially dependent on the bandgap energy.^{48,49} These findings could be verified using TRPL measurements in a future study.

The temperature dependence of the integrated PL intensity for both samples is shown in Fig. 3(b). The rate of thermal quenching was largest for sample B. The cause of the thermal quenching may be related to material defects in the SL or thermal escape of excitons from

the electron miniband to the conduction band of InSb which then recombine non-radiatively.⁴² Further PL investigations (4 K) are required for reliable extraction of the activation energies of the non-radiative mechanism due to the multiple peaks observed in these samples and the uncertainty of peak fitting methods at high temperatures, but this is beyond the scope of the present work.

The 77 K PL spectra of Samples A and B are shown in Figs. 4(a) and 4(b), respectively. The maximum PL intensity of sample A was nearly 8.5 times larger than that of sample B indicating an increase in non-radiative recombination centers in sample B, which corroborates the earlier observed high defect density by XRD measurements.⁵⁰ Surprisingly, the peak position of sample B is redshifted by ~ 10 meV compared to sample A (Table II), while previous experimental studies^{50,51} reported a compressive strain-induced blue shift of the peak wavelength. The origin of this redshift is likely related to the difference in period thickness or composition measured by XRD above as this can greatly affect the peak wavelength. Both samples show a primary peak (P_1) and two shoulders (P_2 and P_3) at larger energies. To understand the origins of these peaks, Gaussian approximation was used to

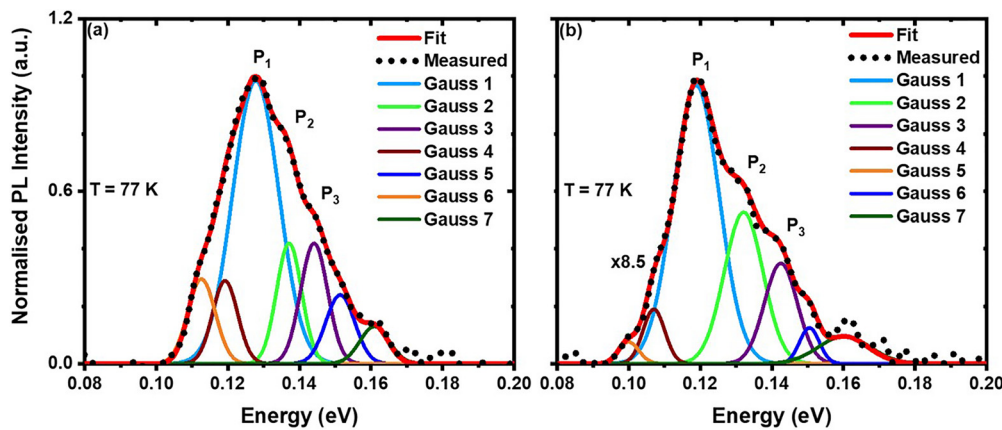


FIG. 4. PL profiles at 77 K with fitted Gaussians and envelope function for (a) sample A and (b) sample B.

TABLE II. PL peak positions for samples A and B.

Sample	Peak (P_n)	Center (eV)	Height (arb. units)	FWHM (eV)
Sample A	1	0.1278	0.99	0.014
	2	0.1371	0.42	0.0076
	3	0.1441	0.42	0.0082
Sample B	1	0.1188	0.97	0.014
	2	0.1321	0.53	0.012
	3	0.1428	0.36	0.01

fit the PL spectra as depicted in Fig. 4. The largest peak, P_1 (related to Gauss 1), corresponds to the primary e_1-hh_1 transition with an FWHM of 14 meV which is consistent with a previous report.⁵² Gauss 2 and 3 were fitted to Peaks P_2 and P_3 , respectively, while Gauss 4–7 were added to ensure a good agreement between the measured profile and the resulting envelope function.

The parameters used to fit Gauss 1–3 are given in Table II.

Peaks P_2 and P_3 are unrelated to the second heavy hole or split-off bands as these transitions occur at much higher energies. A more likely explanation is provided by Weisbuch *et al.*⁵³ who proposed that growth islands of ~ 1 ML thickness can form at the interfaces of barriers and wells in multi-quantum well heterostructures. This gives rise to uncertainty in the well width which, when applied to the well-known equation for energy levels in an infinite quantum well, gives the following expression for the uncertainty:

$$\Delta E_1 = \Delta L_z \frac{h^2}{4m^* L_z^3}, \quad (2)$$

where ΔE_1 is the energy uncertainty, ΔL_z is the well width uncertainty, h is the Planck's constant, m^* is the effective mass, and L_z is the well width. By taking the uncertainty in well width to be half the lattice constant and the effective mass to be a weighted average of the InAs and GaSb effective masses the energy uncertainty can be calculated to be around 0.01 eV. This is in good agreement with the variation between Gauss 1, 2, and 3 (Table II). The distance between successive

peaks is larger for sample B suggesting the energy uncertainty is larger for this sample. This is in agreement with XRD measurements, which indicate the period thickness, and therefore well width, is smaller for this sample, which will increase the energy uncertainty. This result is supported by the findings of Kim *et al.*⁴¹ who report a high level of intermixing at the IFs of Ga-containing T2SLs, particularly when an intentional InSb IF is grown, using atom probe tomography (APT) and high-resolution (scanning) transmission electron microscopy (HR(S)TEM).

A possible explanation for the presence of Gauss 4–7 is the formation of sub-monolayer quantum dots (QDs) at the IFs as InGaSb QDs have been reported to emit in the LWIR.^{54,55} Furthermore, the growth kinetics are favorable for the preferential formation of InGaSb QDs due to the respective diffusion lengths of Ga and In. An informative future study would be to verify the existence of growth islands and QDs using HRTEM.

In order to determine the uniformity or otherwise of the as-grown films, we investigated the influence of PL spot position along the substrate surface on the PL profiles of the samples. 77 K PL mapping was performed at different points along the substrate surface of each sample as shown in Fig. 5.

As can be seen, the optical behavior of sample A is largely independent of position, unlike sample B which shows a large variation in both the shape of the PL profile and the maximum intensity. Interestingly, peaks P_1 , P_2 , and P_3 of sample A are still observable at positions which closely correlate with those observed in Fig. 4. This substrate dependent behavior may be due to the disparity in thermal expansion of the GaSb and GaAs substrates⁵⁶ or the presence of defects in sample B. Nomarski Microscopy, shown in Fig. 5(a') and (b'), was performed at selected positions on each sample. It is clear that a relatively high density of defects and dislocations is present in sample B in comparison with A. This is consistent with the larger XRD FWHM and decreased PL intensity earlier discussed. The non-uniformity of film growth of sample B, which is visible on the substrate surface, also supports the non-uniform PL behavior observed in Fig. 5(b). The structural and optical non-uniformity of Sample B raises concerns for the scale-up from single-pixel to FPA applications for

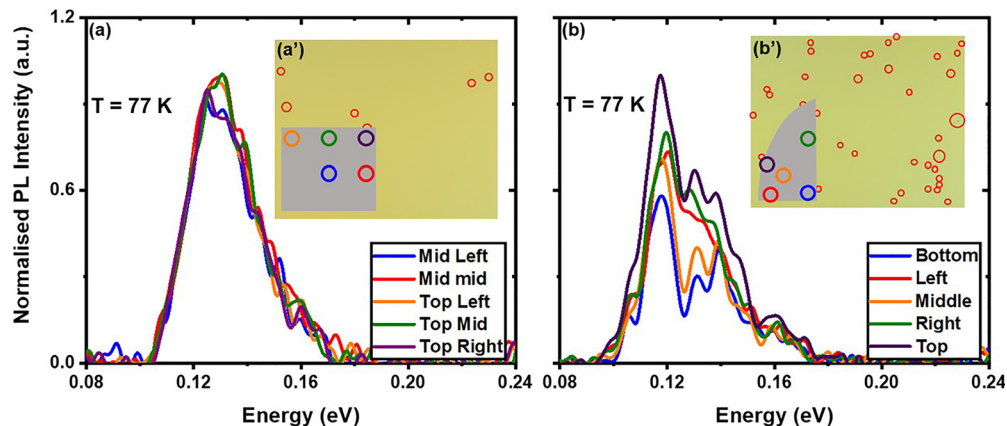


FIG. 5. PL mapping for selected spots on (a) sample A and (b) sample B. Representative Nomarski micrographs from (a') sample A and (b') sample B. Insets provide a schematic of approximate PL positions.

devices grown on GaAs substrates. These results suggest that the IMF array alone is not sufficient for the growth of high-quality, high uniformity T2SL wafers. Instead, it is important to employ the IMF array alongside a thick, strain-balanced buffer layer to mitigate the degradation in material quality brought about by the non-native substrate.

In conclusion, LWIR InAs/GaSb T2SLs have been grown on GaSb and GaAs substrates. In the latter case, an IMF array was used to grow a 500 nm GaSb buffer layer on the GaAs substrate. The GaSb substrate has been shown to promote the growth of high-quality SL layers with superior optical properties compared to the SL on GaAs. PL measurements suggest the presence of sub-monolayer QDs at the interfaces of both samples which could be confirmed by HRTEM in a future study. The non-uniformity issues related to the GaAs substrate must be overcome to allow the scale up to FPA applications. Further studies are also required to investigate the impact of the non-native substrate on diode performance.

All the authors acknowledge the financial support provided by Sêr Cymru National Research Network in Advanced Engineering and Materials. M. Delmas also acknowledges Marie Skłodowska-Curie Grant Agreement No. 743521.

DATA AVAILABILITY

The data that support the findings of this study are available from the corresponding author upon reasonable request.

REFERENCES

- ¹Directive 2011/65/EU of the European Parliament and of the Council, see https://ec.europa.eu/environment/waste/rohs_eee/index_en.htm for “RoHS-Restriction” (last accessed January 05, 2021).
- ²G. A. Sai-Halasz, R. Tsu, and L. Esaki, *Appl. Phys. Lett.* **30**, 651 (1977).
- ³A. Rogalski, P. Martyniuk, and M. Kopytko, *Appl. Phys. Rev.* **4**, 031304 (2017).
- ⁴A. Rogalski, P. Martyniuk, and M. Kopytko, *Prog. Quantum. Electron.* **68**, 100228 (2019).
- ⁵E. A. Plis, *Adv. Electron.* **2014**, 1–12.
- ⁶M. Razeghi, B. M. Nguyen, P. Y. Delaunay, E. K. Huang, A. Pour, P. Manukar, and S. Bogdanov, *Proc. SPIE* **7467**, 181 (2009).
- ⁷E. R. Youngdale, J. R. Meyer, C. A. Hoffman, F. J. Bartoli, C. H. Grein, P. M. Young, R. H. Miles, and D. H. Chow, *Appl. Phys. Lett.* **64**, 3160 (1994).
- ⁸C. H. Grein, P. M. Young, M. E. Flatté, and H. Ehrenreich, *J. Appl. Phys.* **78**, 7143 (1995).
- ⁹H. Mohseni, V. Litvinov, and M. Razeghi, *Phys. Rev. B* **58**, 15378 (1998).
- ¹⁰A. Khoshakhlagh, S. Myers, H. Kim, E. Plis, N. Gautam, S. J. Lee, S. K. Noh, L. R. Dawson, and S. Krishna, *IEEE J. Quantum Electron.* **46**, 959 (2010).
- ¹¹P. C. Klipstein, E. Avnon, Y. Benny, R. Fraenkel, A. Glzman, S. Grossman, O. Klin, L. Langoff, Y. Livneh, I. Lukomsky, M. Nitzani, L. Shkedy, I. Shtrichman, N. Snapi, A. Tuito, and E. Weiss, *Proc. SPIE* **9070**, 256 (2014).
- ¹²A. D. Hood, A. J. Evans, A. Ikhlassi, D. L. Lee, and W. E. Tennant, *J. Electron. Mater.* **39**, 1001 (2010).
- ¹³B.-M. Nguyen, D. Hoffman, P.-Y. Delaunay, E. K. Huang, and M. Razeghi, *Proc. SPIE* **7082**, 33 (2008).
- ¹⁴N. Gautam, H. S. Kim, M. N. Kutty, E. Plis, L. R. Dawson, and S. Krishna, *Appl. Phys. Lett.* **96**, 231107 (2010).
- ¹⁵D. Z. Ting, C. J. Hill, A. Soibel, S. A. Keo, J. M. Mumolo, J. Nguyen, and S. D. Gunapala, *Appl. Phys. Lett.* **95**, 023508 (2009).
- ¹⁶K. Michalczewski, P. Martyniuk, L. Kubiszyn, C.-H. Wu, Y.-R. Wu, J. Jurenczyk, A. Rogalski, and J. Piotrowski, *IEEE Electron Device. Lett.* **40**, 1396 (2019).
- ¹⁷K. Michalczewski, Ł. Kubiszyn, P. Martyniuk, C. H. Wu, J. Jurenczyk, K. Grodecki, D. Benyahia, A. Rogalski, and J. Piotrowski, *Infrared Phys. Technol.* **95**, 222 (2018).
- ¹⁸K. Michalczewski, T.-T. Tsai, C.-S. Wu, and P. Martyniuk, *Proc. SPIE* **10830**, 217 (2018).
- ¹⁹K. Michalczewski, T. Y. Tsai, P. Martyniuk, and C. H. Wu, *Bull. Pol. Acad. Sci., Chem.* **67**, 141 (2019).
- ²⁰R. Müller, V. Gramich, M. Wauro, J. Niemasz, L. Kirste, V. Daumer, A. Janaszek, J. Jurenczyk, and R. Rehm, *Infrared. Phys. Technol.* **96**, 141 (2019).
- ²¹R. Müller, M. Haertelt, J. Niemasz, K. Schwarz, V. Daumer, Y. V. Flores, R. Ostendorf, and R. Rehm, *Micromachines* **11**, 1124 (2020).
- ²²S. A. Pour, B. M. Nguyen, S. Bogdanov, E. K. Huang, and M. Razeghi, *Appl. Phys. Lett.* **95**, 173505 (2009).
- ²³B. M. Nguyen, D. Hoffman, E. K. W. Huang, S. Bogdanov, P. Y. Delaunay, M. Razeghi, and M. Z. Tidrow, *Appl. Phys. Lett.* **94**, 223506 (2009).
- ²⁴D. Benyahia, Ł. Kubiszyn, K. Michalczewski, J. Boguski, A. Kęblowski, P. Martyniuk, J. Piotrowski, and A. Rogalski, *Nanoscale Res. Lett.* **13**, 196 (2018).
- ²⁵S. Huang, G. Balakrishnan, and D. L. Huffaker, *J. Appl. Phys.* **105**, 103104 (2009).
- ²⁶E. Plis, J. B. Rodriguez, G. Balakrishnan, Y. D. Sharma, H. S. Kim, T. Rotter, and S. Krishna, *Semicond. Sci. Technol.* **25**, 085010 (2010).
- ²⁷M. J. Hobbs, F. Bastiman, C. H. Tan, J. P. R. David, S. Krishna, and E. Plis, *Proc. SPIE* **8899**, 17 (2013).
- ²⁸C. G. Burguete, D. Guo, P. Jurczak, F. Cui, M. Tang, W. Chen, Z. Deng, Y. Chen, M. Gutierrez, B. Chen, H. Liu, and J. Wu, *IET Optoelectron.* **12**, 2 (2018).
- ²⁹X. B. Zhang, J. H. Ryoo, R. D. Dupuis, A. Petschke, S. Mou, S. L. Chuang, C. Xu, and C. Hsieh, *Appl. Phys. Lett.* **88**, 072104 (2006).
- ³⁰A. Jasik, I. Sankowska, J. Ratajczak, A. Wawro, D. Smoczyński, K. Czuba, and M. Wzorek, *Curr. Appl. Phys.* **19**, 120 (2019).
- ³¹Z. Deng, D. Guo, C. G. Burguete, Z. Xie, J. Huang, H. Liu, J. Wu, and B. Chen, *Infrared. Phys. Technol.* **101**, 133 (2019).
- ³²E. Delli, V. Letka, P. D. Hodgson, E. Repiso, J. P. Hayton, A. P. Craig, Q. Li, R. Beanland, A. Krier, R. J. Marshall, and P. J. Carrington, *ACS Photonics.* **6**, 538 (2019).
- ³³E. Delli, P. D. Hodgson, M. Bentley, E. Repiso, A. P. Craig, Q. Lu, R. Beanland, A. R. J. Marshall, A. Krier, and P. J. Carrington, *Appl. Phys. Lett.* **117**, 131103 (2020).
- ³⁴D. H. Chow, R. H. Miles, J. R. Söderström, and T. C. McGill, *Appl. Phys. Lett.* **56**, 1418 (1990).
- ³⁵D. H. Chow, *J. Vac. Sci. Technol. B* **8**, 710 (1990).
- ³⁶R. H. Miles, D. H. Chow, J. N. Schulman, and T. C. McGill, *Appl. Phys. Lett.* **57**, 801 (1990).
- ³⁷M. Delmas, D. C. M. Kwan, M. C. Debnath, B. L. Liang, and D. L. Huffaker, *J. Phys. D: Appl. Phys.* **52**, 475102 (2019).
- ³⁸M. Delmas, M. C. Debnath, B. L. Liang, and D. L. Huffaker, *Infrared. Phys. Technol.* **94**, 286 (2018).
- ³⁹M. Gutierrez, D. Araujo, P. Jurczak, J. Wu, and H. Liu, *Appl. Phys. Lett.* **110**, 092103 (2017).
- ⁴⁰X. Li, Y. Zhang, D. Jiang, F. Guo, D. Wang, and L. Zhao, *Superlattices Microstruct.* **104**, 390 (2017).
- ⁴¹H. Kim, Y. Meng, J. L. Rouvière, D. Isheim, D. N. Seidman, and J. M. Zuo, *J. Appl. Phys.* **113**, 103511 (2013).
- ⁴²J. Wu, Z. Xu, J. Chen, and L. He, *Infrared Phys. Technol.* **92**, 18 (2018).
- ⁴³M. Delmas, B. Liang, and D. L. Huffaker, *Proc. SPIE* **10926**, 29 (2019).
- ⁴⁴J.-B. Wang, D. Ding, S. R. Johnson, S.-Q. Yu, and Y.-H. Zhang, *Phys. Status Solidi.* **244**, 2740 (2007).
- ⁴⁵B. C. Connelly, G. D. Metcalfe, H. Shen, and M. Wraback, *Appl. Phys. Lett.* **97**, 251117 (2010).
- ⁴⁶B. C. Connelly, G. D. Metcalfe, H. Shen, M. Wraback, C. L. Canedy, I. Vurgaftman, J. S. Melinger, C. A. Affouda, E. M. Jackson, J. A. Nolde, J. R. Meyer, and E. H. Aifer, *J. Electron. Mater.* **42**, 3203 (2013).
- ⁴⁷P. C. Klipstein, Y. Benny, Y. Cohen, N. Fraenkel, S. Glikman, A. Glzman, I. Hirsh, L. Langof, I. Lukomsky, I. Marderfeld, B. Milgrom, M. Nitzani, D. Rakhamilevich, L. Shkedy, N. Snapi, I. Shtrichman, E. Weiss, and N. Yaron, *J. Electron. Mater.* **49**, 6893 (2020).
- ⁴⁸Y. Aytac, B. V. Olson, J. K. Kim, E. A. Shaner, S. D. Hawkins, J. F. Klem, M. E. Flatté, and T. F. Boggess, *J. Appl. Phys.* **118**, 125701 (2015).

- ⁴⁹J. S. Blakemore, *Semiconductor Statistics*, 1st ed. (Dover Publications, New York, 1962).
- ⁵⁰M. Korkmaz, B. Arıkan, Y. E. Suyolcu, B. Aslan, and U. Serincan, *Semicond. Sci. Technol.* **33**, 035002 (2018).
- ⁵¹C. P. Kuo, S. K. Vong, R. M. Cohen, and G. B. Stringfellow, *J. Appl. Phys.* **57**, 5428 (1985).
- ⁵²S. Suchalkin, G. Belenky, S. P. Svensson, B. Laikhtman, S. Smirnov, L. C. Tung, and S. Bandara, *J. Appl. Phys.* **110**, 043720 (2011).
- ⁵³C. Weisbuch, R. Dingle, A. C. Gossard, and W. Wiegmann, *Solid State Commun.* **38**, 709 (1981).
- ⁵⁴O. Gustafsson, A. Karim, Q. Wang, J. Berggren, C. Asplund, J. Y. Andersson, and M. Hammar, *Infrared. Phys. Technol.* **59**, 89 (2013).
- ⁵⁵R. Liu, Y. Zhong, L. Yu, H. Kim, S. Law, J.-M. Zuo, and D. Wasserman, *Opt. Express* **22**, 24466 (2014).
- ⁵⁶H. Detz, *Electron. Lett.* **51**, 1455 (2015).